Study Of Convective Heat Transfer And Pressure Drop Characteristics Inside Shell And Semi-Circular Tubes Heat Exchanger

M.M. Ellaban , M.A. Abdelrahman, M.R. Salem, M.A. Moawed, K.M. Elshazly

Mechanical Engineering Department, Faculty of Engineering at Shoubra, Benha University

Abstract. Different Methods are used to enhance heat transfer in shell and tube heat exchanger. The present work examines numerically the effect of splitting the internal tubes for a shell and tubes heat exchanger on its hydrothermal performance. The effect of the spacing between the semi-circular tubes (SCTs) to the tube diameter; spacing ratio (δ) in addition to the shell-side fluid inlet temperature and flow rate are the main parameters. ANSYS 15 with 3D fluid flow is used for the modeling and simulation of the present study. The Results indicate that splitting the internal tubes of a shell and tube heat exchanger significantly increases the rate of heat transfer and flow resistance in the shell-side when compared with that in the heat exchangers of circular tubes. In addition, the shell-side average Nusselt number, friction factor and hydrothermal performance index (HTPI) increase with increasing the SCTs spacing ratio. Finally, the shell and SCTs heat exchanger of $\delta = 0.5$ have the highest *HTPI*; 1.87 at the higher shell-side flow rate.

Keywords : Numerical; Convection; Semi-circular tubes; Heat exchanger; Nusselt Number; Friction.

Nomenclatures

A	Area, m²
Cp	Specific heat, J/kg. °C
d	Diameter, m
f	Fanning friction factor
$\bar{h}$	Average convection heat transfer coefficient, W/m². °C
k	Thermal conductivity, W/m. °C
L	Length, m
ṁ	Mass flow rate, kg/s
P	Pressure, Pa
Q	Heat transfer rate, W
T	Temperature, °C
u	Axial velocity, m/s
$\dot{V}$	Volume flow rate, m³/s
S	Spacing; the distance between the bases of two adjacent SCTs, m
x, y, z	Cartesian coordinate Components
u, v, w	Instantaneous velocity component in x, y, z directions

Dimensionless Groups

$\overline{Nu}$	Average Nusselt number
Pr	Prandtl number
Re	Reynolds number
St	Stanton number

Greek Letters

Δ	Differential
μ	Dynamic viscosity, kg/m. s
ρ	Density, kg/m³
δ	the ratio between the SCTs spacing and the tube diameter

1. INTRODUCTION

Heat transfer is a branch of science that is existed in a lot of applications around us. Every industrial process, power station, air conditioning and combustion processes have a transfer of thermal energy from a hot-side fluid to a cold-side one to exploit it in a process ,which helps us in usual life. The heat exchanger with its different shapes is a device, which is responsible of transferring energy from one fluid mass to another. Minimizing the allowed area for the heat transfer in addition to the pressure drop play the main factor for getting

the optimum performance of heat exchangers to achieve the heat transfer requirements [1].To get the desired the heat exchanger dimensions at more economic pumping power, a lot of methods have been introduced. Those improvements methods can be sorted into active and passive methods. Numerous researches were conducted on changing shapes and cross-sectional area of the internal tubes in the heat exchangers to improve their thermal performance, and consequently intents in cost and material. Ota et al. [2] and Merker and Hanke[3] experimentally estimated the heat transfer characteristics from an elliptic shaped pipe. They estimated that the elliptic tube has a higher performance than the circular one in specific flow conditions. Khan et al. [4]conducted experiments for elliptic tubes carry cooling water in cross array with hot air. The results referred to that the Nusselt number was found to change in power law relation with Re. In another research, tubes of cam configuration were investigated experimentally for forced convective heat transfer for cross flow by Nouri-Borujerdi and Lavasani[5]for different attack angles. The results exhibited that the superior heat transfer coefficient could be attained at attack angle of 90°. Nada et al. [6]computationally and experimentally checked the heat transfer attributes for SCT in cross flow at different angles and various orientations. The results conducted that when the flat surface faces the flow gave a lower average Nusselt number than the curved surface faced the flow. Derby et al. [7]in experimental way Freon R134a is tested for the condensation in triangular, square, and semicircular mini-channels with the same hydraulic diameter. At lower mass fluxes, the results showed an improvement of the triangle and square geometries. Zhang et al. [8]investigated the condensation of a steam on elliptic twisted horizontal tubes. It was shown that the condensation coefficient was augmented with the raise of the tube ellipticities.El Gharbi et al. [9]performed numerical investigations to simulate the heat exchange and the pressure loss attributes and compatibility of a cross-flow heat exchanger using staggered tube bank type with various geometries; circular, elliptic and wind-shaped tubes. It was indicated that the circular tube shape is worse compared with the other shapes for Re > 1.5x10^4, and the elliptic shape is the best for Re > 2.3x10^4.Kumar et al. [10]numerically studied the flow and convection heat transfer attributes around a SCT placed in a confined channel. The results demonstrated that the flow was steady, as two symmetric vortices has formed behind a SCT, for the range of Re < 69.Et al[11] experimentally and numerically analyzed the thermal performance attributes in a heat exchanger of circular and elliptical tubes.

In this study, different tubes-orientations in addition to baffle cut ratios were used. It was obvious that the elliptical profile is responsible for a higher hydrothermal performance.Gupta et al. [12]conducted study on the characteristics of the thermal performance in shell and elliptic tube heat exchanger. The results revealed that when the ratio between the major and minor axis was less than 1, the velocity increased in both sides of the heat exchanger by 9.8% and 15.3%, respectively, and heat transfer coefficient increased by 14.5% and 20.2%, respectively.Cheng et al. [13]examined the stream resistance in addition to the heat exchange attributes in twisted oval tubes of different twisted pitch and flattening ratios. The results indicated that the heat transfer and the pumping power increased with increasing the tubes flatting and decreasing the twisted pitch ratio. From previous, it is cleared that the changing in geometry of tubes for heat exchanger lead to good results in heat transfer characteristics.

In the current work, plain pipes are split into two SCTs. Different spacing's between the bases of each SCTS are tested at different shell-side operating conditions.

2. Semi-Circular Tubes

Knowledge of the heat transfer and pressure drop attributes are the main factors which affect choosing suitable and most relevant heat exchanger .The proposed enhancement method in the present work is using SCTs instead of complete circular ones, which enlarges the surface area of the heat transfer. A schematic representation of a SCT with main geometrical parameters is shown in Fig. 1.
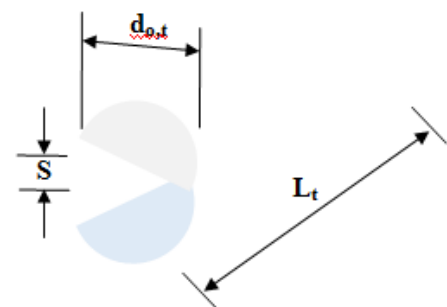

Fig. 1: Basic geometry of a semi-circular Tube

•The SCT can be geometrically described by Outer diameter of the tube ($d_{o,t}$), Spacing (S) and Length of the tube (L_t). A schematic representation of shell and SCTs with main geometrical parameters is shown in Fig. 2.
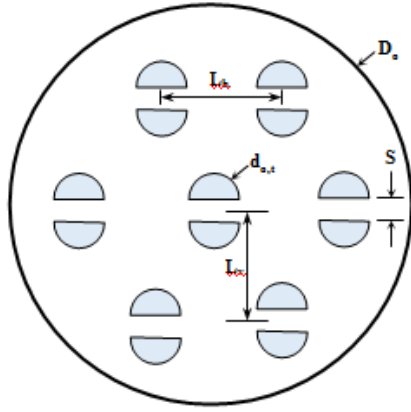
Fig. 2: A schematic representation of shell and semi-circular tubes.

A dimensionless parameter is proposed in the current study is the spacing ratio, δ, to expresses the ratio between the SCTs spacing and the tube diameter, defined as follows;

$$\delta = \frac{S}{d_{o,t}} \qquad (1)$$

3. Modeling Details

In this study, the thermal performance of a horizontal heat exchanger of shell and SCTs (Fig. 3) is numerically simulated for different shell-side operating conditions and different spacing ratios (Table 1). The properties of water are defined as constants in the ANSYS-database. In addition, standard κ-ε and standard wall functions are applied during the model design. The desired mass flow rates and inlet temperatures values are assigned to the inlet port of the heat exchanger as indicated in Table 1. Zero-gauge pressure is assigned to the outlet port, to get the pressure drop between inlet and outlet. The inlet velocity is assumed to be uniform without slip condition is considered to all surfaces. Also, no heat flux boundary condition is considered to the shell outer wall, assuming the shell is completely isolated.
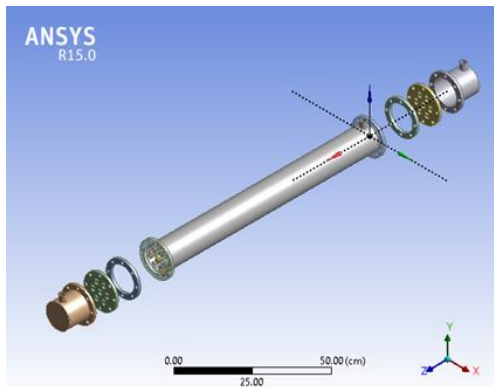

Fig. 3: Assembly of the shell and semi-circular tube heat exchanger.

Table 1: Design and geometric parameters.

Parameter	Value or range
Shell-side flow rate (L/min)	6.02–18.37 ($3293.3 \leq Re_{sh} \leq 17473.4$)
Tubes total flow rate (L/min)	42.64
Tubes inlet temperature (°C)	50
Shell inlet temperature (°C)	15, 20, 25 ($4.9 \leq Pr_{sh} \leq 7.3$)
Tube inner diameter, m	0.0145
Tube outer diameter, m	0.016
Tube length, m	0.95
Shell diameter, m	0.1
Number of complete circular tubes	7
Spacing ratio	0.15, 0.25, 0.5

Mesh generation is performed using ANSYS, in which the shell and tubes volumes are meshed using tetrahedral method. The effect of the mesh size is firstly tested. The medium mesh, with 462336 nodes and 2261950 elements, is generated for the circular tubes case. While these numbers increase for the SCTs case. The used governing equations of the flow are modified respect to the conditions of the present case. Since the problem is supposed to be steady, parameters which are depended on time are omitted from the governing equations. The resulting equations are;

Conservation of mass: $\dfrac{\partial u}{\partial x} + \dfrac{\partial v}{\partial y} + \dfrac{\partial w}{\partial z} = 0$ (2)

x-momentum

$$\rho\left(u\frac{\partial u}{\partial x} + v\frac{\partial u}{\partial y} + w\frac{\partial u}{\partial z}\right) = \rho g_x - \frac{\partial p}{\partial x} + \mu\left(\frac{\partial^2 u}{\partial x^2} + \frac{\partial^2 u}{\partial y^2} + \frac{\partial^2 u}{\partial z^2}\right)$$

$$(3)$$

y-momentum:

$$\rho\left(u\frac{\partial v}{\partial x} + v\frac{\partial v}{\partial y} + w\frac{\partial v}{\partial z}\right) = \rho g_y - \frac{\partial p}{\partial y} + \mu\left(\frac{\partial^2 v}{\partial x^2} + \frac{\partial^2 v}{\partial y^2} + \frac{\partial^2 v}{\partial z^2}\right)$$

$$(4)$$

z-momentum:

$$\rho\left(u\frac{\partial w}{\partial x} + v\frac{\partial w}{\partial y} + w\frac{\partial w}{\partial z}\right) = \rho g_z - \frac{\partial p}{\partial z} + \mu\left(\frac{\partial^2 w}{\partial x^2} + \frac{\partial^2 w}{\partial y^2} + \frac{\partial^2 w}{\partial z^2}\right)$$

$$(5)$$

Energy:

$$\rho c_v\left(u\frac{\partial T}{\partial x} + v\frac{\partial T}{\partial y} + w\frac{\partial T}{\partial z}\right) = K\left(\frac{\partial^2 T}{\partial x^2} + \frac{\partial^2 T}{\partial y^2} + \frac{\partial^2 T}{\partial z^2}\right) + \varphi$$

$$(6)$$

In Eq. (6), φ is the dissipation function that can be calculated from;

$$\varphi = \mu\left[2\left(\frac{\partial u}{\partial x}\right)^2 + 2\left(\frac{\partial v}{\partial y}\right)^2 + 2\left(\frac{\partial w}{\partial z}\right)^2 + \left(\frac{\partial v}{\partial x} + \frac{\partial u}{\partial y}\right)^2 + \left(\frac{\partial w}{\partial y} + \frac{\partial v}{\partial z}\right)^2 + \left(\frac{\partial u}{\partial z} + \frac{\partial w}{\partial x}\right)^2\right]$$

$$(7)$$

4. Data Reduction

Heat transfer rates for Shell-side (Q_{sh}) and tubes-side (Q_t) are calculated as follows;

$$Q_{sh} = \dot{m}_{sh} C_{p,sh}\left(T_{sh,o} - T_{sh,i}\right) \qquad (8)$$

$$Q_t = \dot{m}_t C_t (T_{t,i} - T_{t,o}) \qquad (9)$$

The average heat transfer rate is estimated as;

$$Q_{ave} = (Q_{sh} + Q_t)/2 \qquad (10)$$

Heat Balance Deviation is as follows;

$$\Delta Q_{ave}(\%) = \frac{|Q_t - Q_{sh}|}{Q_{ave}} * 100 \qquad (11)$$

The maximum deviation through all runs is $\pm 3.2\%$. The average heat load is used to evaluate the overall heat transfer coefficient;

$$U_i = \frac{Q_{ave}}{\Delta T_{LM} A_{t,i}} \qquad (12)$$

The logarithmic mean temperature difference is defined for counter flow as follows;

$$\Delta T_{L.M} = \frac{(T_{t,i} - T_{sh,o}) - (T_{t,o} - T_{sh,i})}{\ln\left[\frac{T_{t,i} - T_{sh,o}}{T_{t,o} - T_{sh,i}}\right]} \qquad (13)$$

By neglecting the conduction resistance of the tube wall and fouling, the overall thermal conductance can be expressed in terms of the thermal resistances as follows;

$$\frac{1}{U_i A_{t,i}} = \frac{1}{\overline{h}_{sh} A_{s,o}} + \frac{1}{\overline{h}_t A_{t,i}} \qquad (14)$$

The tube-side average heat transfer coefficient is calculated usingDittus-Boelter[14]correlation for Nusselt number as follows;

$$\overline{h}_t = \frac{\overline{Nu}_t k_t}{d_{t,h}} = 0.023 \, Re_t^{0.8} Pr_t^{0.4} * \frac{k_t}{d_{t,h}} \qquad (15)$$

Then, the average Nusselt number for the shell-side fluid, $\overline{Nu}_{sh}$, is obtained as follows;

$$\overline{Nu}_{sh} = \frac{\overline{h}_{sh} d_{sh,h}}{k_{sh}} \qquad (16)$$

5. Model Verification

To validate the present model, the results of the CFD are compared with Dittus-Boelter[14],(Eq. 17),and Gnielinski[15],(Eq. 18), for the shell-side average Nusselt number, and with Filonenko[16],(Eq. 19),for the shell-side friction factor, using a heat exchanger of complete circular tubes. The inlets temperatures and flow rates are varied as indicated in Table 2. The results of these comparisons are illustrated in Fig. 4.
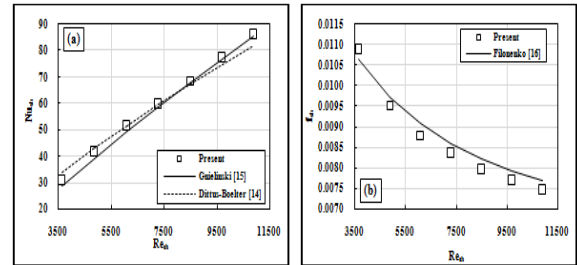
$$\overline{Nu}_{sh} = 0.023 \, Re_{sh}^{0.8} Pr_{sh}^{0.3} \qquad (17)$$

$$\overline{Nu}_{sh} = \frac{\frac{f_{sh}}{2}(Re_{sh} - 1000)Pr_{sh}}{1 + 12.7\sqrt{\frac{f_{sh}}{2}}\left(Pr_{sh}^{2/3} - 1\right)}\left[1 + \left(\frac{d_{sh,h}}{L_{sh}}\right)^{2/3}\right] \qquad (18)$$

$$f_{sh} = 0.25(1.82 \log Re_{sh} - 1.64)^{-2} \qquad (19)$$

Table 2: Verification operating conditions.

| Parameter	Value or range
Shell-side flow rate (L/min)	6–18
Tubes total flow rate (L/min)	42
Tubes inlet temperature (°C)	50
Shell inlet temperature (°C)	20

Fig. 4: The results of comparisons; (a) Average

Nusselt number, (b) Fanning friction factor.

It is clear that the experimental results for both heat transfer and friction factor calculations are in good relevance with previous studies with maximum deviations of $\pm 3.1\%$ and $\pm 2.8\%$ for $\overline{Nu}_{sh}$ and f_{sh}, respectively. This good agreement in comparisons reveals the accuracy of the CFD model.

6. Results

6.1 Effect of Semi-Circular Tubes Spacing

In this analysis, three SCT spacing ratios (0.15, 0.25 and 0.5) are simulated for the indicated operating conditions in Table 1. Fig. 5 shows a sample of the results ($T_{sh, i} = 20°C$) for $\overline{Nu}_{sh}$ and f_{sh} due to varying the spacing ratio at different flow rates of the shell-side fluid. While Figs. 6 and 7 demonstrate the obtained velocity and temperature contours at the midpoint of the heat exchanger, respectively.
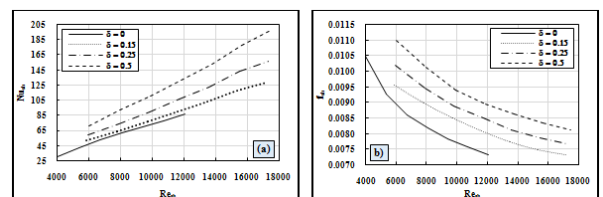
Fig. 5: The effect of SCT spacing ratio at different Shell-side Reynolds numbers ($T_{sh, i} = 20°C$); (a) Average Nusselt number, (b) Fanning friction factor.

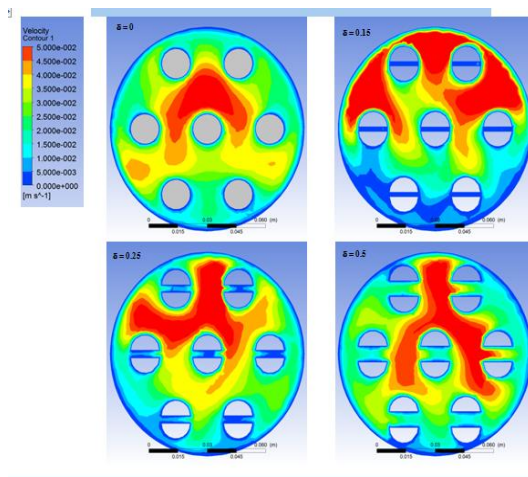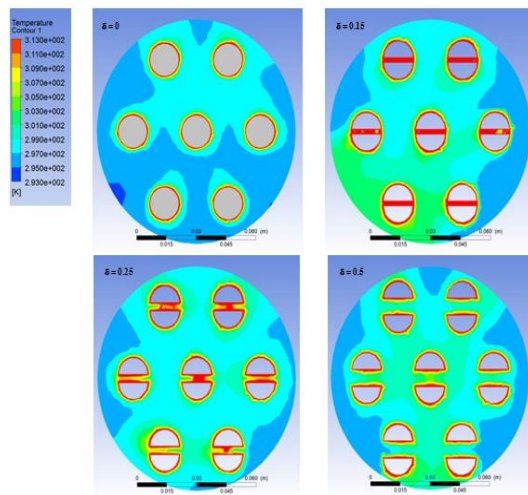**Fig. 6: Shell-side velocity contours at different SCT spacing ratios ($T_{sh,\,i} = 20°C$).**

Fig. 7: Shell-side temperature contours at different SCT spacing ratios ($T_{sh,\,i} = 20°C$).

It is clearly shown in Fig. 5 that the shell-side average Nusselt number and friction factor are higher than that of the circular tubes case, and they increase with increasing the SCT spacing ratio. Compared with the circular tubes case, the shell-side average Nusselt number increases by 47.2% and 115.3%, while the shell-side friction factor increases by 9.1% and 23.8% at δ = 0.15 and δ = 0.5, respectively, at the same sell-side flow rate and inlet temperature. This can be attributed to increasing the shell-side flow turbulence level around the internal tubes with increasing the SCT spacing ratio as shown in Fig. 6. It is obvious that at the smallest spacing between the SCTs, the flow velocity beside their bases is very small where the tubes throttle the flow at this region, while this is accompanied with a larger distance between the tubes, which decreases the overall pressure drop. On contrary, increasing the SCTs spacing ratio permits a higher flow velocity between the their bases, which augments the heat transfer rate, and also this is accompanied with a lower distance between the internal tubes, which

increases the shell-side flow resistance, and consequently enhances the flow mixing and improves the heat transfer rate. This is very clear in the temperature contours in Fig.7.

6.2 Effect of Shell-Side Operating Conditions

In this analysis, three shell side inlet temperatures and seven flow rates are simulated for the indicated operating conditions in Table 1. Fig. 8shows a sample of the results ($δ = 0.15$) for $\overline{Nu}_{sh}$ and f_{sh}.

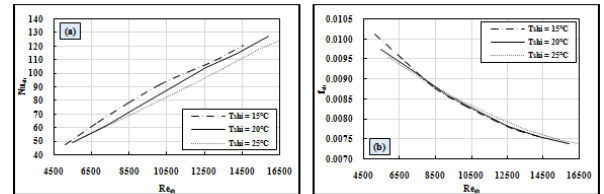Fig. 8: The effect of shell-side operating conditions at $δ = 0.15$; (a) Average Nusselt number, (b) Fanning friction factor**.**

It is clear from all runs that as the inlet temperature of the shell-fluid flow increases, $\overline{Nu}_{sh}$ decreases at the same Re_{sh}. This can be attributed to the decrease in Prandtl number with increasing the water temperature. In addition, it can be seen that the effect of the flow inlet temperature on the friction factor is nearly insignificant. This can be returned to the lower effect of viscosity variation compared with the inertia force. Additionally, it is noticeable that increasing Re_{sh} augments $\overline{Nu}_{sh}$. This is due to increasing the fluctuations level and fluid layers mixing around the internal tubes by increasing Reynolds number. On contrary, increasing Re_{sh} reduces f_{sh}, which can be returned to that momentum forces overcome viscous forces as Re_{sh} increases.

6.3 Hydrothermal Performance Index

To be a successful heat transfer enhancement tool, the rise in the convective heat transfer given due splitting the internal tubes in the shell-side of the heat exchanger should be higher than the rise in the fluid flow resistance. Thus, the combined hydrothermal performance index (HTPI) is determined using St_{sh} and f_{sh} ratios [17], [18] that are estimated using the values obtained for SCTs and circular tubes, as follows;

$$HTPI = \frac{St_{sh,SCT}/St_{sh,cir}}{\left(f_{sh,SCT}/f_{sh,cir}\right)^{1/3}} \qquad (20)$$

This HTPI combines the effects of the thermal improvement and the increase in the pressure drop [18]. Over the studied range of shell-side inlet temperatures, the average *HTPI* is

estimated and the results are demonstrated in Fig. 9 for different SCTs spacing ratios and shell-side flow rates.
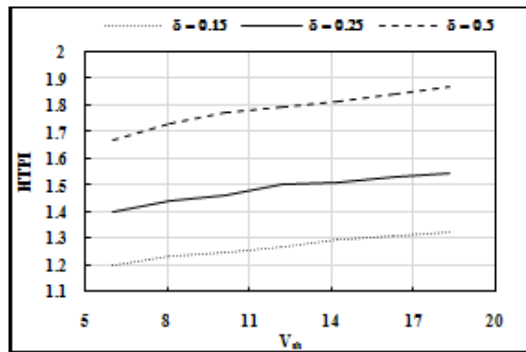

Fig. 9: Variation of the average HTPI at different SCTs spacing ratios.

It is obvious that the *HTPI* is more than unity for all ranges of investigated parameters. It is clear that the *HTPI* increases with increasing the spacing ratio and shell-side Reynolds number. Over the studied range of operating conditions, spacing ratio of $\delta = 0.5$ provides the maximum values of the *HTPI*; 1.67 and 1.87 at lower and higher shell-side flow rates, respectively.

Conclusions

The current study numerically examines the thermal performance attributes of a horizontal shell and SCTs of counter flow configuration. The SCTs-spacing ratios and operating conditions of the shell-side are the main parameters throughout this study. In the simulation runs, the investigated operating parameters are $3293.3 \leq Re_{sh} \leq 17473.4$, $4.9 \leq Pr_{sh} \leq 7.3$, and $0 \leq \delta \leq 0.5$. According to the obtained results, the following conclusions can be expressed:

- Splitting the internal tubes of a shell and tube heat exchanger significantly increases the rate of heat transfer and flow resistance in the shell-side when compared with that in the heat exchangers of circular tubes.
- The shell-side average Nusselt number, friction factor and HTPF increase with increasing the SCTs spacing ratio.
- There is a slight increase in shell-side average Nusselt number with decreasing the shell-side inlet temperature, while its effect on the shell-side friction factor can be ignored.
- Shell and SCTs heat exchanger of δ = 0.5 have the highest *HTPI*1; 1.87 at the higher shell-side flow rate.

REFERENCES

[1] U. U. REHMAN, Heat Transfer Optimization of Shell-and-Tube, Goteborg, Sweden: CHALMERS UNIVERSITY, 2011.

[2] T. Ota, S. Aiba, T. Tsuruta and M. Kaga, "Forced Convection Heat Transfer from an Elliptic Cylinder of Axis Ratio 1:2," Bull. JSME, vol. 26, pp. 262–267, 1983.

[3] Hanke and G. Merker, "Heat Transfer and Pressure Drop on the Shell-Side of Tube-Banks having Oval-Shaped Tubes," International Journal of Heat and Mass Transfer, vol. 29 (12), pp. 1903–1909, 1986.

[4] M. G. Khan, A. Fartaj and Ting, "An Experimental Characterization of Cross-Flow Cooling of Air via an In-Line Elliptical Tube Array," International Journal of Heat and Fluid Flow, vol. 25, pp. 636–648, 2004.

[5] Lavasani and A. Nouri-Borujerdi , "Experimental Study of Forced Convection Heat Transfer from a Cam Shaped Tube in Cross Flows," International Journal of Heat and Mass Transfer, vol. 50, pp. 2605–2611, 2007.

[6] S. A. Nada, H. El-Batsh and M. Moawed, "Heat Transfer and Fluid Flow Around Semi-Circular Tube in Cross Flow at Different Orientations," Heat Mass Transfer, vol. 43, pp. 1157–1169, 2007.

[7] M. Derby, H. J. Lee, Y. Peles and M. K. Jensen, "Condensation Heat Transfer in Square, Triangular, and Semi-Circular Mini-Channels," International Journal of Heat and Mass Transfer, vol. 55, pp. 187–197, 2012.

[8] L. Zhang, S. Yang and H. Xu, "Experimental Study on Condensation Heat Transfer Characteristics of Steam on Horizontal Twisted Elliptical Tubes," Applied Energy, vol. 97, pp. 881–887, 2012.

[9] N. E. Gharbi, A. Kheiri, M. E. Ganaoui and R. Blanchard, "Numerical Optimization of Heat Exchangers with Circular and Non-Circular Shapes," Thermal Engineering, vol. 6, pp. 194–203, 2015.

[10] A. Kumar, A. Dhiman and L. Barany, "Fluid Flow and Heat Transfer Around a Confined Semi-Circular Cylinder: Onset of Vortex Shedding and Effects of Reynolds and Prandtl Numbers," International Journal of Heat and Mass Transfer, vol. 102, pp. 417–425, 2016.

[11] Raju, J. B. B. Rao and V. Ramachandra, "Numerical and Heat Transfer Analysis of Shell and Tube Heat Exchanger with Circular and Elliptical Tubes," International Journal of

Mechanical and Materials Engineering, vol. 11:6 (1), 2016.

[12] P. Gupta, A. K. Sharma and ". Raj Kumar, "Thermal Design of Shell and Tube Heat Exchanger Using Elliptical Tube," International Journal of Engineering and Manufacturing Science, ISSN 2249-3115, vol. 7 (1), pp. 47-50, 2017.

[13] J. Cheng, Z. Qian and Q. Wang, "Analysis of Heat Transfer and Flow Resistance of Twisted Oval Tube in Low Reynolds Number Flow," International Journal of Heat and Mass Transfer, vol. 109, pp. 761–777, 2017.

[14] F. Dittus and L. Boelter, ""Heat transfer in Automobile Radiators of the Tubular Type",," vol. 2, University of California Publications in Engineering, 443461, [Lawrence, A. E], 1930.

[15] V. Gnielinski, ""New Equations for Heat and Mass Transfer in Turbulent Pipe and Channel Flow"," Int Chem Eng., vol. 16, pp. 359–368., 1976.

[16] G. Filonenko, ""Hydraulic Resistance of Pipes "," (Hydraulischer Widerstand Von Rohrleitungen), Teploenergetika, vol. 1 (4), pp. 40-44., 1954.

[17] H. Al-Kayiem, A. B. Ekhwan and L.N. Muhi, ""Augmentation of Ribs Turbulators Height on the hydrothermal performance of Double Pipe Heat Exchanger"," J Eng Sci Technol., vol. 12 (2), pp. 548–563., 2017.

[18] M. Salem, M. Eltoukhy, R. Ali and K.M. Elshazly, ""Experimental Investigation on the Hydrothermal Performance of a Double-Pipe Heat Exchanger Using Helical Tape Insert"," International Journal of Thermal Sciences, vol. 124, pp. 496-507., 2018.